Experimental Brain Research (2023) 241:2311–2332
https://doi.org/10.1007/s00221-023-06684-9

RESEARCH ARTICLE

A computational model of motion sickness dynamics during passive self-motion in the dark

Aaron R. Allred[1] · **Torin K. Clark**[1]

Received: 18 April 2023 / Accepted: 4 August 2023 / Published online: 17 August 2023

Abstract

Predicting the time course of motion sickness symptoms enables the evaluation of provocative stimuli and the development of countermeasures for reducing symptom severity. In pursuit of this goal, we present an observer-driven model of motion sickness for passive motions in the dark. Constructed in two stages, this model predicts motion sickness symptoms by bridging sensory conflict (i.e., differences between actual and expected sensory signals) arising from the observer model of spatial orientation perception (stage 1) to Oman's model of motion sickness symptom dynamics (stage 2; presented in 1982 and 1990) through a proposed "Normalized innovation squared" statistic. The model outputs the expected temporal development of human motion sickness symptom magnitudes (mapped to the Misery Scale) at a population level, due to arbitrary, 6-degree-of-freedom, self-motion stimuli. We trained model parameters using individual subject responses collected during fore-aft translations and off-vertical axis of rotation motions. Improving on prior efforts, we only used datasets with experimental conditions congruent with the perceptual state (i.e., adequately provided passive motions without visual cues) to inform the model. We assessed model performance by predicting an unseen validation dataset, producing a Q^2 value of 0.86. Demonstrating this model's broad applicability, we formulate predictions for a host of stimuli, including translations, earth-vertical rotations, and altered gravity, and we provide our implementation for other users. Finally, to guide future research efforts, we suggest how to rigorously advance this model (e.g., incorporating visual cues, active motion, responses to motion of different frequency, etc.).

Keywords Vestibular · Sensory conflict · Predictive modeling · Spatial disorientation · Orientation perception

Introduction

Significance of motion sickness

Beyond self-ambulation on Earth, motion sickness pervades all modes of human transportation (e.g., automobiles, boats, trains, airplanes, and spacecraft). Often experienced by passive observers, motion sickness symptoms are most universally characterized by sweating, increases in salivation, dizziness, and headache ultimately leading to sopite syndrome, nausea, and/or vomiting (Lackner 2014). Such symptoms spanning from slight discomfort to prolonged incapacitation have motivated decades of empirical studies and modeling efforts.

Concerning the terrestrial environment, early motion sickness models and severity studies were developed with seasickness as the primary motivation. While still applicable today, a renewed interest in motion sickness has arisen alongside the advent of autonomous automobiles, deep space exploration, and commercial space travel. In the context of the space environment, most astronauts experience motion sickness upon transitioning to a microgravity environment from Earth and upon returning to Earth following extended exposure to microgravity (Davis et al. 1988; Oman 1987). Affecting 60–80% of space travelers (Heer and Paloski 2006) and coined 'space motion sickness (SMS)' or 'space adaption syndrome (SAS),' this mode of motion sickness is not thought to be a unique diagnostic entity to terrestrial motion sickness (Lackner and DiZio 2006). Because SMS/SAS poses significant operational and performance decrements to crew members in the first days of travel (Ortega et al.

Communicated by Bill J Yates.

✉ Aaron R. Allred
aaron.allred@colorado.edu

[1] Smead Department of Aerospace Engineering Sciences, University of Colorado-Boulder, Boulder, CO, USA

2019), more effective countermeasures to motion sickness must be developed to improve crew health and performance during future NASA exploration class missions.

Stemming from these applications, across various motion and environmental stimuli, there exists a principal need to construct the foundation of a broadly applicable, validated motion sickness model. This development will further enable the construction and evaluation of motion sickness countermeasures, which otherwise may not always be intuitive (e.g., in some instances, the addition of 'countermeasures', such as the addition of visual cues and various behavioral approaches, may result in more severe motion sickness). Enabling the formulation of a quantitative computational model of the dynamics of motion sickness symptoms, there currently exists both a strong conceptual understanding of the cause and contributions to motion sickness and relevant empirical datasets.

Sensory conflict and models of self-orientation perception

For the last half century, the most prominent theoretical explanation for motion sickness stems from sensory conflict theory, though alternatives exist (Bos 2011; Riccio and Stoffregen 1991) which are not necessarily mutually exclusive. Sensory conflict, the difference between 'sensed' and the brain's centrally 'expected' cues, particularly in regard to vestibular cues, has been proposed to drive motion sickness (Oman 1982, 1990; Reason and Brand 1975). While other sensory pathways and associated conflicts (e.g., somatosensory, visual, etc.) could contribute to motion sickness, motion sickness is often believed to occur in individuals without functioning vestibular systems, though there is some evidence to the contrary (Golding 2015; Johnson et al. 1999; Murdin et al. 2015). Physiologically, the neural representation of this conflict may exist in the brainstem and cerebellum (Laurens 2012; Oman and Cullen 2014).

The sensory conflict theory for motion sickness offers an explanation for the development of motion sickness symptoms for all known forms of motion sickness from both physical motion (e.g., car sickness, sea sickness, air sickness, etc.), apparent/illusory motion (e.g., simulator sickness), and changing environmental stimuli (e.g., space motion sickness). Apart from this crucial function of driving motion sickness, sensory conflict is thought to play a more fundamentally necessary role of driving perception of self-motion. This has been computationally captured via the Luenberger observer framework (Luenberger 1971), particularly for passive motions where sensory conflict is often most present (Wolpert et al. 1995). Over the last thirty years, models of self-orientation perception have been developed with variously defined sensory conflict signals.

A prominent perceptual model of self-orientation perception is the 'Observer' model (Clark et al. 2019; Merfeld et al. 1993; Newman 2009; Zupan et al. 2002). In the Observer model, to produce central perception of self-motion and orientation, sensory measurements for the semicircular canals and otoliths of the vestibular system are processed to yield three sensory conflict signals (angular velocity conflict, linear acceleration conflict, and gravito-inertial force (GIF) directional conflict); all have an associated weighting gain which, when multiplied by the conflicts, updates the state estimates (i.e., self-motion and orientation perception, see Appendix A1 for more information). Because the Observer model uses its internal estimates to inform each other (e.g., its internal estimate of angular velocity is used to perceive gravity's direction in the head-centered reference frame [i.e., tilt]), it is often described as using a 'multi-sensory integration' approach. Multi-sensory integration is implemented via 'internal models' which are thought to take the form of learned neural relationships of kinematic and sensory dynamics.

Another relevant model is the subjective vertical conflict (SVC) model (Bos and Bles 1998). This model uses 'frequency segregation:' gravity is hypothesized to be 'sensed' from the central processing of the otolith sensory measurements via a low-pass filter in an Earth-fixed reference frame, computed from the perceived rotation rates via Mayne's principal (Mayne 1974). While the SVC model does not rely on a truly 'sensed' cue to generate the SVC, this conflict is used to drive perception of linear acceleration through a gain and integration. Bos and Bles defined the SVC as the difference between the low-pass filtered otolith cues (i.e., the pseudo-'sensed' gravity vector) and the internal estimate of this signal (i.e., the 'expected' gravity vector; see Appendix A1).

With the goal of bridging motion stimuli and motion sickness in humans, these models of self-orientation perception, driving sensory conflict, have either been used (in the case of the SVC model) or proposed (in the case of an Observer model) as the first 'stage' in various dynamical models of the development of motion sickness symptoms (Oman 1982, 1990).

Computational models of motion sickness dynamics

It has previously been proposed that the same processing of sensory information (multi-sensory integration, internal models, and sensory conflict) used for spatial orientation perception is also critical for producing motion sickness. With sensory conflict as an input, various computational models of motion sickness dynamics have been developed. Using motion sickness data captured during upright vertical oscillations across both frequency and amplitude (O'Hanlon and McCauley 1974), the SVC model with a

downstream motion sickness stage was tuned to achieve peak motion sickness incidence for sinusoidal oscillations at around 0.16 Hz for upright, vertical motion across amplitudes. Because O'Hanlon and McCauley used motion sickness incidence (MSI) to quantify motion sickness severity across subject populations, the SVC motion sickness model estimates MSI by feeding the conflict through a Hill function and subsequent 2nd-order low-pass filter (Bos and Bles 1998). Later, Turan et al. presented a six degree-of-freedom motion implementation of this model aboard high-speed vessels (Turan et al. 2009).

Relying on a single vestibular conflict to drive motion sickness, the SVC model contains multiple supposed limitations (Khalid et al. 2011a, b). These include: the inability to capture different frequency effects between earth-vertical and upright earth-horizontal translations (Donohew and Griffin 2004; Golding et al. 2001; Griffin and Mills 2002a; O'Hanlon and McCauley 1974) and faster onset of symptoms for earth-horizontal motions (Golding et al. 1995). A proposed remedy to these limitations, a subjective vertical-horizontal (SVH) conflict model was developed (Khalid et al. 2011a, b; Khalid et al. 2011a, b). Critically, the SVH conflict model was tuned to additionally match the frequency response for Earth-horizonal translations observed empirically (Donohew and Griffin 2004) by incorporating a second conflict as input to the motion sickness stage. This 'horizontal conflict' is similar to the subjective vertical conflict but instead relies on components of the gravito-inertial force vector normal to gravity in order to estimate MSI. Fundamentally the same as SVC model, a coined 'six degree-of-freedom' model was developed (Kamiji et al. 2007) and augmented with the addition of active head-tilt control (Wada et al. 2018) and later, with the addition of visual information (Wada et al. 2020). This chain of model development has been centered around predicting car sickness.

Beyond these iterations of the SVC model, Irmak et al. (2022) constructed a temporal model based on Oman's heuristic model of motion sickness. Oman iteratively proposed a heuristic model of motion sickness (Oman 1982, 1990) to capture the temporal dynamics of motion sickness severity from a scalar input comprised the vestibular sensory conflict signal. Considering augmentations to Oman's proposal in 1990 (such as input scaling) Irmak et al. (2022)'s model of motion sickness severity estimates, the time course of motion sickness symptoms where the model output is a continuous Misery Scale (MISC) estimate. The MISC is a unidimensional, qualitative 11-point scale that roughly corresponds to the progression of motion sickness symptoms, where an increase in the magnitude of the MISC score corresponds to an increase in the severity of motion sickness symptoms (Bos et al. 2005). Notably, this model did not contain a perceptual processing stage and instead assumed the conflict vector to be proportional to the acceleration stimulus.

Limitations of existing models

The aforementioned models of motion sickness have been structured around the hypothesis that sensory conflict from spatial orientation perception also drives motion sickness. Despite this theoretical foundation, these models have manipulated the spatial orientation stage to produce desirable estimates of motion sickness severity (despite not revalidating the spatial orientation stage in terms of predicting spatial orientation perception). For example, in the Bos- and Bles SVC-driven motion sickness models, the effect of oscillatory motion frequency (i.e., motion sickness peaking around 0.16 Hz) of the emetic response was tuned by modifying parameters in the perceptual stage of the model (by adjusting the feedback gain driving perception of head acceleration), thus not guaranteeing a valid model of self-orientation perception [the validity of resultant perceptions have been recently explored for various motion paradigms (Groen et al. 2022, p. 20; Irmak et al. 2023)]. Critically, the tuned parameters in the perceptual stage imply that adaption to a changing gravity magnitude occurs in seconds rather than days. For others (Wada et al. 2018, 2020), no validation of the perceptual stages have occurred. In fact, other works have found the validity of the perceptual stage to be inconsistent with empirical data (Yunus et al. 2022a; b). In the case of Irmak et al. (2022), the spatial orientation perception stage was omitted (using acceleration as a proxy for sensory conflict), precluding the model from predicting motion sickness from arbitrary motions where different combinations and amplitudes of sensory conflict are present.

Beyond not containing a validated spatial orientation perception stage, the augmented 'six degree-of-freedom' models (Wada et al. 2018, 2020) include pathways that suggest the central nervous system has direct access to the actual/ground-truth acceleration and angular velocity state vectors when modeling active head tilts. This model violates our current understanding of the neural processes governing how active motion commands (efference copies), forward models, and active motion sensory feedback (reafferent signals) are integrated into motion perception. While it is likely that their proposed pathways were intended to serve as proxies for more detailed active pathways, it is unlikely that the resultant sensory conflicts produced by their model are generalizable to other motion paradigms.

Further, it is important that the empirical data of motion sickness severity used to tune or optimize a model is congruent with the perceptual model used to produce sensory conflict. Both the presence of active motions (e.g., postural control, in which the brain is aware of commanded self-motion, informing the expectation of sensory measurements)

and visual cues (either congruent with a fixed Earth reference frame or some moving reference frame e.g., inside of a ship cabin) have been found to affect motion sickness. Active motion augments sensory conflict due to the presence of an efference copy, forward internal model, and expected reafferent signals modifying the expected vestibular sense. Active head movements have been found to significantly affect motion sickness symptoms (Johnson and Mayne 1953; Lackner and Graybiel 1987). Moreover, experiments where subjects (particularly subjects' heads) are not well-constrained may provide the vestibular system with additional self-motion stimuli not accounted for when fitting models to experimental data. Illustrating these points, less-restrained (low-backrest seating) conditions have been found to produce more severe motion sickness symptoms compared to more restrained (high-backrest seating) during identical whole-body lateral oscillations (Mills and Griffin 2000), likely due to differences in vestibular stimulation with less restraint.

The presence of visual cues (either Earth-fixed or subject-fixed) also augments the expected vestibular sense, changing the sensory conflict experienced by the subject (and may even introduce additional 'visual sensory conflict' terms influencing motion sickness symptoms). To this point, motion sickness severity (resulting from primarily physical motion stimuli) has been found to be affected in the presence of visual cues (Bos et al. 2005), and simulator-driven motion sickness is worsened by visual scenes incongruent with vestibular cues (Kolasinski 1995). Therefore, it is critical that models of motion sickness based on sensory conflict are conceptually congruent with the experience of the subject in the experiment(s) to which the model is tuned/fit.

Contrary to this requirement, Bos and Bles used a perceptual model based on passive motion without visual cues (and additionally but less crucially, without somatosensory cues) while the data used to tune the model (O'Hanlon and McCauley 1974) allowed subjects to keep their eyes open in a lit cabin (and subjects' heads were not strictly restrained). When devising their SVH model, Khalid et al. used data of horizontal oscillations (Donohew and Griffin 2004), where subjects were instructed to use active postural control to align themselves with the perceived upright while performing a visual search task. In all cases, this presence of active posture control and visual cues is not present in the perceptual stage of the SVH model. Furthermore, in the Donohew and Griffin study, the motion device trajectory (which was input into the model) ignores the substantial self-motion of the subject's postural control, such that the empirical stimulation to the vestibular system differs from that input into the model.

Efforts that do not use a validated spatial orientation stage (via manipulating parameters or by not modeling pathways) no longer offer a rigorous evaluation of the hypothesis that the same neural processing mechanism that drives spatial orientation perception is also driving motion sickness. This also holds if the spatial orientation stage and the empirical data used to fit/tune are incongruent, implying that the spatial orientation perception stage of the model is incomplete. Of additional note is that none of these modeling efforts use multiple datasets or motion paradigms to fit/tune their models, so it is unclear if these models should generalize to arbitrary 6-degree-of-freedom motion stimuli.

Given the evidence of brainstem and cerebellar neurons that respond analogously to the hypothesized sensory conflict signals [i.e., signaling is greatly reducing during active motions, where the brain can better expect sensory signals, as opposed the same motion experienced passively; (Brooks and Cullen 2009; Jamali et al. 2019; Roy and Cullen 2004)], we have chosen to leverage the Observer spatial orientation model, and implement its integration with the Oman emetic pathway model. Our goal is to tune and validate this comprehensive model implementation using several motion paradigms that are definitively congruent with the mechanisms in the model (i.e., passive motion without visual cues).

Motion sickness model formulation

We propose using a motion sickness severity model driven by sensory conflict resulting from a perceptual model validated across several motion paradigms (i.e., the "Observer" model for spatial orientation perception during passive motions). This choice reflects the decision to build a computational model based on sensory conflict theory. Parameters of the Observer model were consistent with the implementation of Clark et al. (2019) and not further modified here. The downstream motion sickness dynamic pathways are based on Oman's heuristic model (1982, 1990). With passive motion over time as an input, the model produces predictions of motion sickness symptoms over time. The overarching framework of this model is depicted in Fig. 1.

The Observer model achieves its main function, producing estimates of self-motion and self-orientation, by first simulating the peripheral dynamics of the vestibular organs. For both the semicircular canals and otolith organs, transfer function representations of how angular velocity and GIF are transduced produce afferent signals, which are then compared to central expectations of these signals. These central expectations are generated through internal, central models of vestibular dynamics and kinematic relationships. The differences between actual and expected sensory measurements yields sensory conflict. For the passive Observer model depicted in Fig. 1, central perceptions of angular velocity, gravity, and linear acceleration are driven by weighted sensory conflict.

Oman's model of motion sickness severity takes some weighted and rectified sensory conflict signal, h, and passes

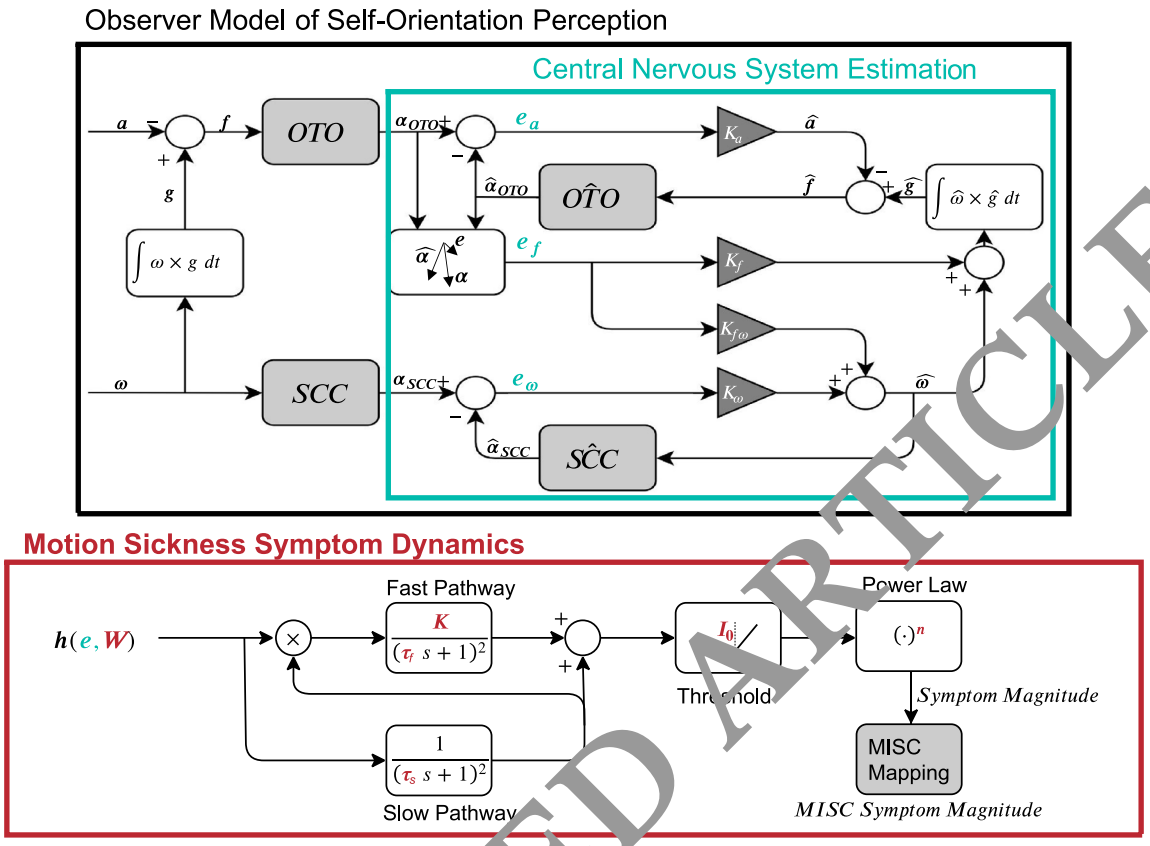

Fig. 1 The two-stage model of motion sickness developing from physical motion. Stage 1 (the spatial orientation stage) is the observer model, where sensory conflict drives internal state estimates of self-motion. Sensory conflicts from stage 1 are fed into stage 2 (the motion sickness symptom dynamics) as proposed by Oman (1982, 1990)

this time-varying scalar through the motion sickness symptom dynamics. The sensory conflict stems directly from the central nervous system estimate within the Observer model of self-orientation perception. The motion sickness symptom dynamics first comprised slow and fast-pathway leaky integrators in the form of 2nd-order low-pass filters. The Oman gain, K, dictates the gain ratio between the fast and slow pathways, and the slow pathway acts as an additional gain on the fast pathway [inspired by the hypersensitivity phenomenon (Oman 1990)]. The fast and slow pathways have unique time constants, τ_f and τ_s respectively (with $\tau_f < \tau_s$). The outputs of these two pathways are summed and passed through a 'threshold' function with a dead-zone described by $[0, I_0]$ and inspired by low intensity conflicts resulting in no discernable or delayed motion sickness intensity onset). Following thresholding, motion sickness intensity is output through a power law with exponent n.

Excluding the sensory conflict weights, W (detailed in the following section), there are five trainable free parameters in the motion sickness symptom dynamics. Further, we include a mapping function to map the model output onto the MISC reporting metric.

Processing of sensory conflicts

Within the Observer model, there are nine sensory conflicts for passive motion without visual cues: three vector components for each e_a, e_ω, and e_f (note that while we use a naming convention consistent with Merfeld and colleagues, these conflicts are differences between actual and expected measurements of the vestibular system and are detailed further in Appendix A1). Oman proposed a scalar conflict, h, for input into the motion sickness symptom dynamics stage. As defined by Oman, this scalar conflict, h, should always be positive, with larger values corresponding to greater sensory conflict, which will in turn eventually lead to more severe motion sickness. Oman conceptually suggests that the multi-dimensional and multi-aspect sensory conflict signals should undergo "conflict weighting and rectification" to produce the scalar conflict (also referred to as "weighted sensory conflict (scalar)" or "neural mismatch signal"). To quantitatively implement this concept, we propose a form of h based on the Normalized Innovation Squared (NIS statistic), which has been proposed to drive central adaption to changing environmental stimuli Kravets et al. (2021, 2022):

$$h_k = e_k^T W e_k$$

$$\text{where } e_k = \left[e_{a_x} e_{a_y} e_{a_z} e_{\omega_x} e_{\omega_y} e_{\omega_z} e_{f_x} e_{f_y} e_{f_z} \right]^T \text{ and}$$

$$W = \text{diag}\left(W_{a_x} W_{a_y} W_{a_z} W_{\omega_x} W_{\omega_y} W_{\omega_z} W_{f_x} W_{f_y} W_{f_z} \right). \quad (1)$$

The normalization matrix, shown here as W, is a diagonal matrix of conflict-specific weighting terms because we do not consider cross-conflict contributions (e.g., $e_{a_x} \times e_{a_y}$). Effectively, this process squares each component (ensuring rectification), weights them (accounting for differences in units and contributions to h), and sums them up (yielding a scalar value). While the exact form of the neural circuitry connecting sensory conflict to motion sickness is currently undetermined and remains a theory in premise, the central nervous system would have access to a NIS statistic, or an equivalent constant, based on the sensory conflict signals (without knowing 'ground truth' signals). This approach, where each conflict component contributes toward h, is a general possibility for how each sensory conflict signal may contribute toward the neural mismatch signal. However, in tuning, it may be found that one or more of the weightings within W are zero (or near zero) implying that sensory conflict signal does not contribute to the neural mismatch signal and thus does not drive motion sickness.

It has been proposed that (as a proxy to the neural mismatch signal) simply a signal proportional to the acceleration amplitude alone could be used as a stand in for (Irmak et al. 2022). While this may suffice as a rough approximation for a single-axis translation motion paradigm, the NIS statistic captures specific conflict contributions to motion sickness, enabling prediction of motion sickness for any arbitrary 6-degree-of-freedom passive motion trajectory. To determine how the individual conflict components from the perception processing should be weighted (i.e., values of W) for input into the motion sickness dynamics, weighting terms were fit via an optimization scheme using existing empirical motion sickness data for passive motions in the dark.

Experimental data

For empirical datasets measuring motion sickness, we chose to only consider experiments in which subjects experienced passive motions without active head/torso tilts and no visual cues. We note that this substantially reduced the number of studies that could be leveraged but ensured that the mechanisms included in the model were congruent with the empirical datasets (i.e., we did not include datasets with the head unrestrained, where visual cues were provided, etc. which are not captured in the existing observer perceptual model). There were five datasets identified which matched this criterion (Bijveld et al. 2008; Cian et al. 2011; Dai et al. 2010; Irmak et al. 2021; Leger et al. 1981), with four unique motion paradigms (see Appendix A2 for further details).

As an additional constraint for training this model, we were only able to leverage motion sickness reporting data which contained individual subject responses over time or averaged subject responses over time with all subjects completing the experiment. In the latter case, averaging only *surviving* subjects (while ignoring or otherwise assuming a motion sickness severity for subjects that stop the experiment due to excessive motion sickness) does not faithfully represent the temporal dynamics of motion sickness in the sample population due to selection bias.

The final dataset used for training our model, leveraging upright x-axis (fore-aft) oscillation data (Irmak et al. 2022) and off-vertical axis of rotation (OVAR) data (Dai et al. 2010), consisted of 77 subject response curves across 2 motion paradigms and 5 unique stimuli magnitudes (one at 0.168 Hz and four at 0.3 Hz). There were 26 unique subjects, and the average MSSQ of the subject population is inferred to be in the 42nd and 65th percentile range. While there was an asymmetry between the number of male and female subjects (7F to 19 M), a subject population MSSQ in this range should yield a representative training dataset for the human population despite known differences in motion sickness susceptibility between sexes.

While not leveraged quantitatively to train the model, Leger et al. (1981)'s earth-horizontal rotation data were used to gain insight into the motion sickness dynamics and reduce the total number of free parameters in our model. Specifically, this study found that there were no significant differences between earth-horizontal roll, pitch, and yaw rotations. While the null hypothesis cannot be proven, this finding implies that the following equivalence in corresponding axes is true:

$$h\left(e_{a_y}, e_{a_z}, e_{\omega_x}, e_{f_x}\right) \approx h\left(e_{a_x}, e_{a_z}, e_{\omega_y}, e_{f_y}\right) \approx h\left(e_{a_x}, e_{a_y}, e_{\omega_z}, e_{f_z}\right) \quad (2)$$

A similar inference could be drawn from an extensive ($N = 192$) comparison to y-axis (lateral) and x-axis (fore-aft) oscillations which found no significant difference in illness ratings (from 0.2 Hz to 0.8 Hz) in males (Griffin and Mills 2002a). While notable, this study was not included in this inference because the experiment did not meet the criteria of well-restrained, passive motions (subjects were seated with a low backrest, no head restraint) in the dark (subjects had a fixed cabin view).

Should the weights of the individual conflict components be equal, the above approximate equivalences are always satisfied. This assumption reduces our matrix for weighting sensory conflicts and rectifying them via the NIS statistic from 9 to only 3 free parameters ($\{W_a, W_\omega, W_f\}$),

such that the neural mismatch signal becomes the following (where $\|V\|$ is the 2-norm of the x, y, and z component vector V):

$$h = W_a\|\vec{e_a}\|^2 + W_\omega\|\vec{e_\omega}\|^2 + W_f\|\vec{e_f}\|^2 \quad (3)$$

Predicting reporting metrics

The output of Oman's model of motion sickness symptom dynamics (Oman 1982, 1990) is a magnitude of motion sickness severity (also termed "nausea magnitude estimate" or "subjective discomfort"). This value ranges from zero (corresponding to no motion sickness experienced) to technically infinity (as the motion profile could always be made more intense). However, empirically motion sickness is often best measured using subjective reporting scales with finite bounds (Lawson 2014). We formulated a monotonic mapping to allow motion sickness symptom magnitude predictions from Oman's model of motion sickness symptom dynamics to be converted to MISC symptom magnitude predictions. Ideally, there would be different channels of responses (e.g., separate nausea, emetic, discomfort, etc.) to fully characterize motion sickness symptoms in an individual. However, because the existing motion sickness data we leveraged did not distinguish these channels when querying subjects, a single all-encompassing motion sickness response is incorporated via MISC [consistent with Irmak et al. (2022)'s modeling effort].

In order to map from the continuous output of the Oman model to the MISC reporting metric, a piece-wise linear map with a slope of one and maximum of 10 was established:

$$\mathrm{Map}_{\mathrm{MISC}}(x) = \begin{cases} x, & x < 10 \\ 10, & x \geq 10 \end{cases}. \quad (4)$$

Here x is the input to the reporting mapping function (Oman's magnitude of motion sickness severity). By formulating the model output mapping in this manner, the optimal model parameters were tuned to a time-history of MISC reports provided by subjects on a continuous scale.

Furthermore, two additional reporting mappings were formulated to convert from other reporting metrics to MISC; Dai et al. (2010) used a simplified Pensacola 0–20 scale and Cian et al. (2011) used a six-point, 1–6, scale. Thus, piecewise linear maps were formulated to convert from these scales to MISC. These mappings were constructed by equating anchor points in each of the scales, as outlined by their respective authors, to the MISC equivalent anchor points. All intermediate values were then interpolated between anchor points. These two maps are shown in Fig. 2a and b, respectively (slight modifications to these mappings had only minor impacts upon model fit). Because the Irmak et al. (2022) data were already in a MISC reporting format, no additional mapping was required. While MISC reports are ordinal and qualitative, we treat MISC as a continuous quantitative measure because it has been found to track a general progression of symptoms (Bos et al. 2005, p. 20), and, bolstering this design decision, there is a positive, monotonous relationship between MISC and subjective discomfort (de Winkel et al. 2022). Therefore, all model predictions and fitting were done on a MISC scale, similar to the model proposed by Irmak et al (2022). Consequentially, final model

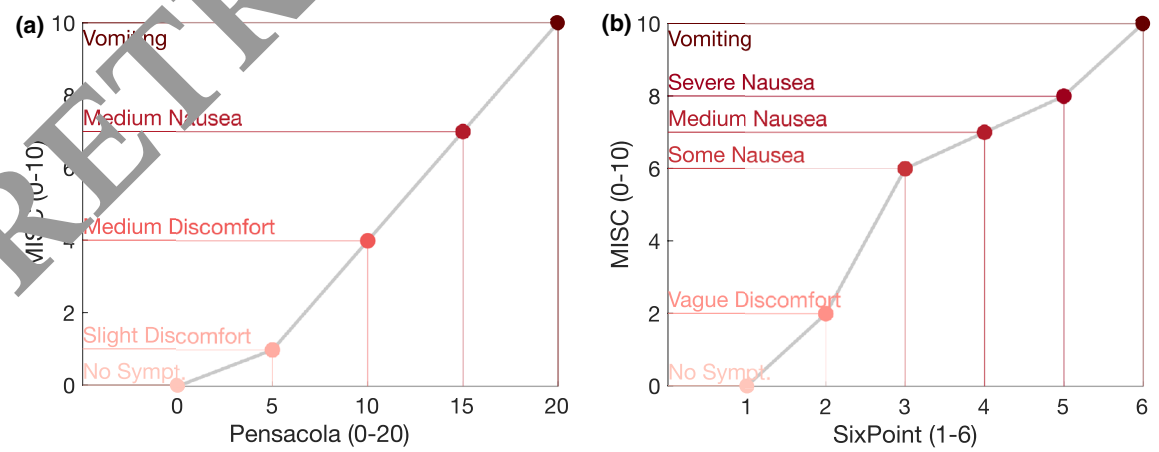

Fig. 2 **a** A piecewise linear map between the Pensacola 0–20 and MISC scales. **b** A piecewise linear map between the six-point 1–6 and MISC scales. These conversions allow data from Dai et al. (2010) and Cian et al. (2011), respectively, to be compared to the model predictions (MISC scale) during training and validation, respectively. The data from Irmak et al. (2022) does not require a mapping because it was recorded using MISC reporting

parameters resulting from the fitting process are dependent on the chosen MISC output, likely a non-linear expression of symptom progression (de Winkel et al. 2022; Reuten et al. 2021).

Cost function

In summary, we aimed to fit the free parameters in the motion sickness model described above by minimizing the differences between model predictions of motion sickness severity over time and those empirically observed in subjects experiencing various motion paradigms. The cost function for minimizing errors in model predictions was formulated to be equally weighted for each subject, regardless of their underlying susceptibility to motion sickness. To accomplish this, each subject's individual mean squared error was normalized by their total measurement reports so that subjects with shorter survival times (i.e., because they experienced excessive motion sickness and did not complete the motion exposure) were not deemphasized during the optimization procedure (and to not overemphasize studies with higher frequency reports). For each subject, a subject mean squared error cost, was calculated, where y_k was reported sickness severity (in MISC units), P_k is the corresponding MISC model prediction at the same discrete point in time (k), m is the total measurements for a given subject, and θ is the set of trainable free parameters in the model: $\theta = \{W_a, W_\omega, W_f, K, \tau_1, \tau_2, I_0, n\}$.

$$J^s_{\mathrm{MMSE}}(\theta; y_{1:m}) = \frac{\sum_{k=1}^{m} \left(P^s_k(\theta) - y^s_k\right)^2}{m}, \tag{5}$$

The full cost function across all subjects (where N is the total number of subjects in an experiment) is the following:

$$J_{\mathrm{MMSE}}(\theta; Y_{1:N}) = \frac{\sum_{s=1}^{N} J^s_{\mathrm{MMSE}}(\theta)}{N}. \tag{6}$$

By minimizing the above cost function, we find $P(\hat{\theta}) = \arg\min_{P(\theta)} J_{\mathrm{MMSE}}(P(\theta); Y_{1:N})$. Because our optimization problem is formulated as a minimum mean squared error estimator, our model optimal solution universally equates to $P(\theta) = E[P(\theta)|Y_{1:N}]$, or the mean human motion sickness symptom dynamics conditioned on all subjects leveraged for training. Thus, we coin our model predictions to be the sample population mean symptom response (SPMSR) as it is conditioned on the measurements gathered from sample data in the literature ($Y_{1:N}$). If a representative, generalizable sample was provided from the collected data, then the model predictions will be equivalent to the population mean symptom response (PMSR), which we refer to from this point forward. This modeling approach produces an expected motion sickness severity for an "average" individual, yielding a useful prediction of the severity of motion sickness with no known insight to individuals' susceptibilities.

Optimization procedure

We present our best-case found solutions, which were found via an optimization routine in MATLAB using *fmincon*. A lower bound was enforced on all optimization parameters of greater than zero to produce real and interpretable solutions. Intermittent results over optimization iterations as well as the initial values, are presented in Appendix A3.

Results

Model optimization results

All instances of optimization (even outside the best results, described here), returned non-zero weighting parameters (W_f, W_a, W_ω), indicating that all three conflict vectors contribute to the neural mismatch signal and thus to the development of motion sickness symptoms. Further, $W_f \gg \{W_a, W_\omega\}$, suggesting the GIF angle conflict contributed the most (though note that the units of the sensory conflicts to which these weights are applied each have different units: g's, rad/s, rad, respectively). The final values of the weights are the following: $W_a = 6.72$, $W_\omega = 11.7$, and $W_f = 562$.

Our best results ($J_{\mathrm{MMSE}} = 3.587$) found I_0 to be near zero (1e−4 [unitless]), similar to the assumptions made by Irmak et al. (2022). However, it is likely that the specific training data used did not contain long enough periods of subthreshold sensory conflict stimuli to uncover a precise value. Final values of the gain ($K = 91.2$), power law ($n = 0.323$), and fast and short time constants ($\tau_f = 74$ s and $\tau_s = 438$ s) differed from, but remained similar to, the median values presented by Irmak et al. (2022) (provided in Appendix A3).

Model prediction results

Model predictions compared to the translational subset of training data revealed similar qualitative fits to those in Irmak et al. (2022), displayed in Fig. 3a. However, the underlying prediction here is a PMSR vs. an individual response, so a direct comparison is not made. Compared to the OVAR subset of training data (Dai et al. 2010), the PMSR is overlaid on individual subject responses in in Fig. 3b. While PMSR reasonably captures the temporal dynamics of training data, individual subjects experienced more or less motion sickness than estimated by the model, as expected.

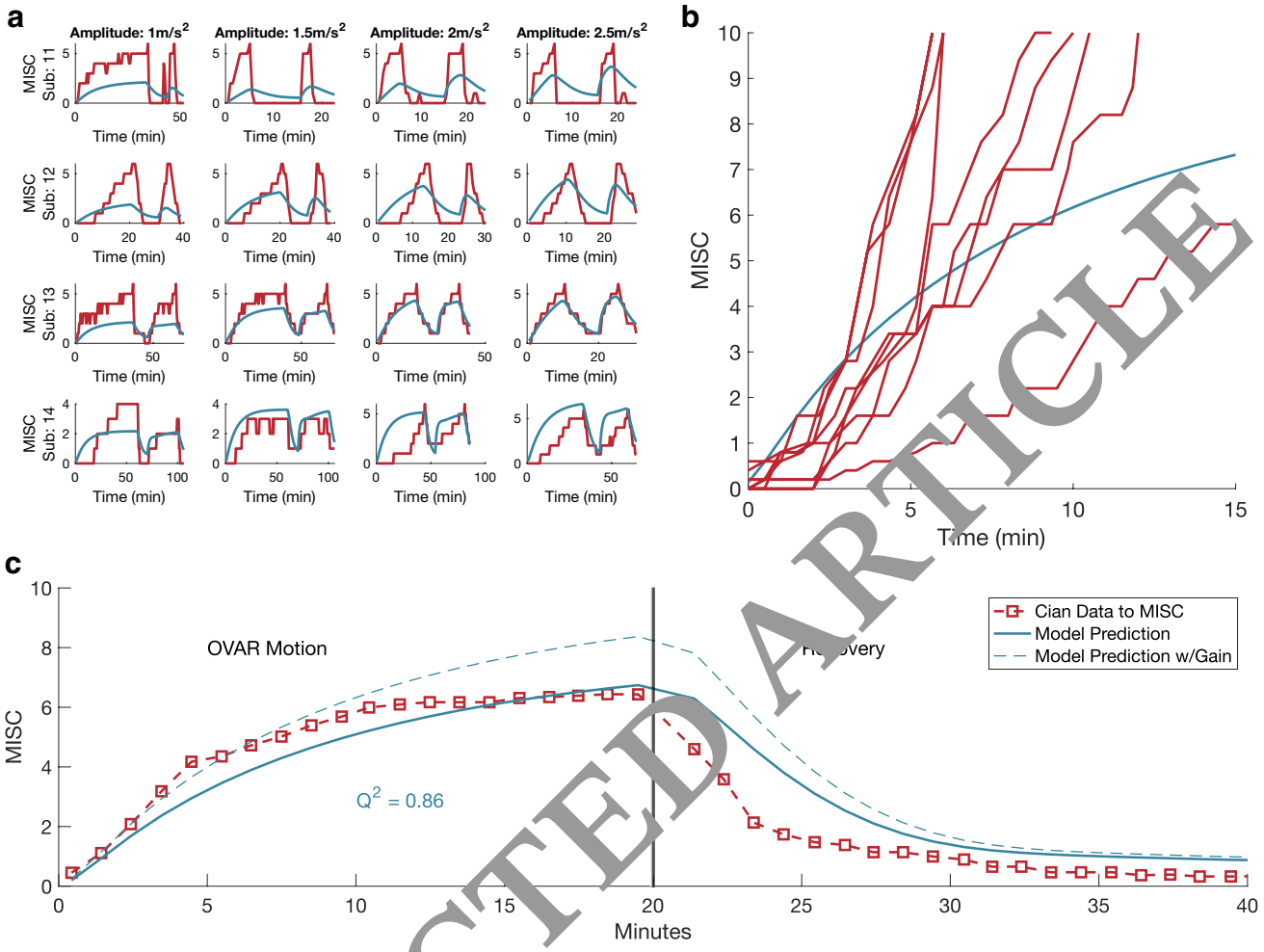

Fig. 3 Model Predictions (displayed in blue) compared to subject data (displayed in red) used for training the model in (**a**, **b**). **a** An example subset of Irmak et al. (2022) subjects (IDs 11–14) across amplitudes (1–2.5 m/s^2). Full results are shown in Appendix A4. The y-axis in all plots is the MISC motion sickness severity scale. **b** All subjects from Dai et al. (OVAR) compared to a single model prediction (all subjects experienced the same motion paradigm over varying lengths of time). **c** Model validation prediction. The red, dashed line is the Cian et al. (2011) mean severity reports of surviving subjects converted from the six-point scale to MISC at the scatter (box symbol) locations. The solid blue line is the model prediction. The dashed blue line is the model prediction with a gain of 1.5 applied to the neural mismatch signal, potentially capturing an unaccounted frequency effect

For a large number of subjects, the temporal dynamics demonstrate first motion sickness 'divergence' (i.e., motion sickness builds more quickly over time) followed by motion sickness 'convergence' (i.e., motion sickness builds more slowly over time). This is both a product of the motion sickness scale used (when mapping to motion sickness severity) and modeling the fast and slow pathways as 2nd-order low-pass filters. For steady conflict stimuli, this leaky integrator first undergoes exponential growth and then eventually converges to a constant value.

Further model evaluations are made on the validation dataset (i.e., unseen during fitting of the model's free parameters), conveyed in Fig. 3c. Forty minutes of model predictions (20 min of OVAR followed by 20 min of recovery without motion) are compared to the mean symptom response of *surviving* subjects from Cian et al. (2011), converted from a six-point scale to MISC (Fig. 2b). The model prediction was evaluated with a Q^2 metric of 0.86 (Q^2 is analogous to R^2, but for predicting unseen data, with good values near 1). While the model captures the temporal dynamics of motion sickness in this unseen dataset, it tends to underestimate the motion sickness severity observed empirically. This result is elaborated upon in the "Discussion".

Additional example simulations

Here we explore additional model predictions for motion paradigms where existing individual motion sickness severity data over time is not known to have been collected during passive motions in the dark (shown in Fig. 4). We cast

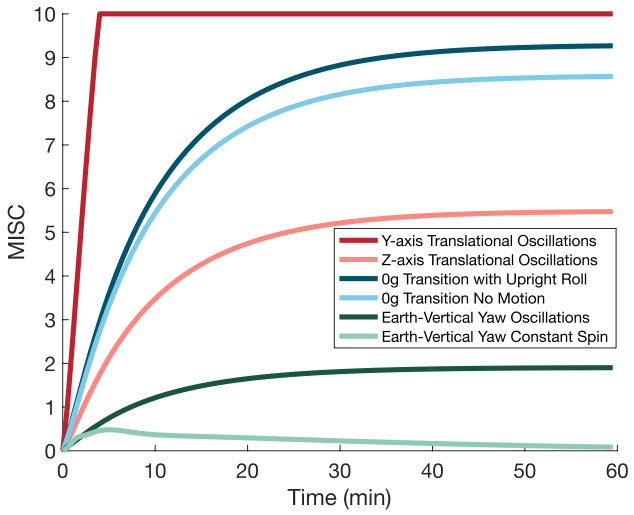

Fig. 4 Model PMSR predictions arising in the presence of various physical and environmental motion stimuli over a 1-h period

predictions for upright y-axis and z-axis oscillatory translations (at 0.3 Hz, peak acceleration of 1 g) to compare earth-horizontal (y-axis) and earth-vertical (z-axis) motions. Earth-vertical yaw motions (both an oscillatory rotation at 0.3 Hz with a peak displacement of 60 degrees and constant spin of 360 deg/s with a 60 s constant ramping up time) are simulated to show how this model predicts symptoms for earth-vertical rotations, a motion paradigm that does not result in any predicted motion sickness in the SVC model. Finally, motion sickness symptoms are simulated for changing environmental stimuli via a gravity transition to 0 g. This changing environmental stimulus was modeled in the Observer model by setting the actual gravity to zero and leaving the internal estimate of gravity (a fixed parameter) at 1 g (i.e., no transient adaptation). Motion sickness symptoms result during both no motion and an upright roll (an oscillatory tilt at 0.3 Hz with a peak displacement of 60 degrees, similar to the yaw motion).

Discussion

We present a computational model predicting the dynamics of MISC symptom magnitudes over time in terms of a population mean symptom response (PMSR). This two-stage model formulates predictions of motion sickness from physical motion stimulation for passive motions in the dark by bridging the Observer model of spatial orientation perception (stage 1) to Oman's model of motion sickness symptom dynamics (stage 2) through a proposed NIS statistic, comprised only the information the central nervous system has access to. Building upon the work of many existing research efforts, we trained our model using data congruent with the perceptual stage of our model and determined the optimal fit of model parameters, finally applying the model to an unseen validation dataset using another motion paradigm.

Model predictions and fit

Because the output of the model is a PMSR for a given motion stimulus and not a prediction of an individual's response, it is not expected that predictions match the shape of the dynamic response on an individual level, hence the differing shape compared to the individual response curves measured by Dai et al. (Fig. 3b). As seen with the validation dataset (Fig. 3c), which captures the mean response of surviving participations from Cian et al. (2011)'s OVAR study, the model prediction does match the temporal dynamics of the ground-truth PMSR (which is desired from our cost function formulation). The Q^2 value of 0.86 on the validation dataset demonstrates this model's ability to match the temporal behavior and suggests that this model provides a true prediction of the PMSR for an unseen motion that can be leveraged to develop countermeasures and evaluate ranked differences in motion sickness for a given motion paradigm. Discussed further in the "Future Model Advancements" section, this model does not account for frequency effects, since no known frequency effects have been noted in the literature for passive motions in the dark. However, we speculate the underestimation of the PMSR compared to the validation dataset may be due to frequency effects for passive motion in the dark. The Irmak et al. (2022) dataset used for training subjected participants to 0.3 Hz motions, and the Dai et al. (2010) datasets subjected participants to 0.167 Hz motions. If a gain of 1.5 is applied to the neural mismatch signal (h) to account for increased population sensitivity to 0.2 Hz conflicts (the spin rate of the Cian et al. OVAR motion paradigm), the model prediction PMSR overshoots the true data near the end of the OVAR motion, before recovery. This is desired since Cian et al. (2011) excluded subjects here that dropped out due to experiencing excessive motion sickness. This bias due to dropouts is not present in the model prediction, such that we would expect the model to overestimate the biased empirical average. Frequency dependent gains are commonly thought to range many orders of magnitude (based on studies concerning sea sickness with either active postural control or visual cues; ISO-2631), thus an unaccounted-for frequency gain around 1.5 is plausible.

The additional model simulations (Fig. 4) reveal that this model predicts that upright y-axis translations are more nauseogenic than upright z-axis translation, a result that is supported by Golding et al. (1995), who found y-axis oscillations to be ~ 2 × more nauseogenic (however, subjects' heads were not restrained, and they conducted a visual search task with visual cues). For earth-vertical yaw, we demonstrate that this model predicts notable motion sickness for upright

yaw oscillations [also observed in the literature, though again with subjects conducting a visual search task (Guedry et al. 1982)] but much less so for constant spin [supported by Leger et al. (1981)]. Finally, this model is capable of predicting motion sickness from changing environmental stimuli as demonstrated by a 1 g to 0 g gravity transition, and motion sickness symptoms are worsened with the addition of physical stimuli (with roll tilts shown here) in the altered gravity environment, consistent with the onset of SMS/SAS.

Contributions advancing upon previously proposed models

Because existing models (Bos and Bles 1998; Khalid et al. 2011a, b; Wada et al. 2020) were tuned using data with experimental conditions not modeled in the perceptual stage of the model, they are not predicting motion sickness from sensory conflict from passive motion paradigms without visual cues via a bottom-up approach. Our implementation allows us to formulate motion sickness symptom predictions from arbitrary motion paradigms for passive motions in the dark. Since the free parameters are trained to one dataset, but then shown to predict another unseen validation dataset reasonably well, it provides some confidence that the model is not overfit, but instead can generalize to arbitrary 6 degrees of free motion stimuli.

Further, this model provides a method of predicting the PMSR, an indicator of how the population will respond to a motion stimulus on average even if the overall form (e.g., variance) of the distribution is unknown. This population-level approach to predicting the time course of motion sickness symptoms allows us to disregard the source of individual differences, which may be present in the motion sickness symptom dynamics stage (Irmak et al. 2022) and/or the perceptual stage (Dai et al. 2003).

Following model predictions of motion sickness, this cohesive model enables further development of countermeasures for motion sickness during passive motions. The results that $W_f \gg \{W_a, W_\omega\}$ suggest that most sickness countermeasures which reduce $|\overrightarrow{e_f}|$, even if this reduction comes at the expense of slightly/moderately increasing $|\overrightarrow{e_a}|$ and/or $|\overrightarrow{e_\omega}|$, may be effective at alleviating the development of symptoms. Further, the non-zero nature of all three weighting terms suggests that all three conflict types may contribute to motion sickness and not just the vector difference conflicts ($\overrightarrow{e_f}$ relates the difference in direction of two vectors, see Appendix A1 for a detailed description). As a final advantage over existing models, this model can produce motion sickness severity predictions from conflict arising from changing environmental stimuli such as experienced by astronauts transitioning between gravity environments and from earth-vertical rotations (Fig. 4). The quantification of symptoms from these additional provocative stimuli (physical, environmental, and a combination of the two) enable the subsequent evaluation of countermeasures for these stimuli.

Limitations of this current model

As previously stated and reemphasized here, the final model parameters and resultant model predictions are conditioned on the training data we used and are appropriate only for modeling passive motions without visual cues. Further, with the inclusion of more motion sickness data from future experiments (particularly those suggested below), it is possible that final parameter values change with the inclusion of more information. Additionally, this model of motion sickness predicts only mean response and ignores individual variability. Individual variability in the development of symptoms has been suggested to be related to the velocity storage time constant (Dai et al. 2003), and modulating this parameter in the perceptual stage as well as modulating sensory noise (not modeled here) are two potential options for incorporating individual variability and quantifying uncertainty bounds around the mean predictions. Since individual susceptibility to motion sickness varies substantially, the model's PMSR prediction may greatly underestimate the motion sickness experienced by a highly susceptible individual and vice versa for an unsusceptible person.

Further, our model does not consider anticipation. Recently, anticipation has been found to affect motion sickness in subjects during experimental trials (Bos et al. 2022). For instance, experiments that provide subjects with visual (Hainich et al. 2021; Karjanto et al. 2018), auditory (Kuiper et al. 2020a; b) and vibrotactile cues (Li and Chen 2022) of motion ahead of motion (~ 1–3 s beforehand) have found varying levels of reductions in reported motion sickness symptoms. Additionally, when subjects are presented repeated motions which do not vary in frequency, direction, or start time, motion sickness is less severe than for more random motions which do vary across these variables (Kuiper et al. 2020a, b). Importantly, the experiments used to train the model all used repeated motions, and thus the model is expected to be biased toward less severe motion sickness predictions for the average subject when presented with motions that are not predictable (e.g., a sum-of-sines motion or an unfamiliar trajectory for a passive observer). It may be expected that less repetitive motions would yield higher severity than the model predictions.

Suggested future experiments

We suggest a number of future studies to rigorously evaluate motion sickness characteristics for future modeling efforts. For all of these recommended future efforts, we urge that individual subject response curves be provided

in the literature or in an online database, rather than just mean scores of surviving subjects. Only providing the latter hinders future modeling efforts by biasing the mean scores toward surviving subject scores (which are lower).

Earth-vertical oscillation motion sickness studies

A host of earth-vertical motion sickness studies could prove useful for isolating individual weights for each conflict type. Earth-vertical translational motions in an upright configuration result in only e_{a_z} sensory conflict. Further, these motions in the supine configuration result in purely e_{a_x} conflict, and lateral recumbent configurations result in purely e_{a_y} conflict. These experiments enable honing the value of W_a (or $W_{ax,y,z}$), which is the primary driver of SMS/SAS symptoms according to this model.

Earth-vertical rotations, while previously studied in a non-provocative constant rotation motion paradigm (Leger et al. 1981), can isolate the rotational conflicts, $e_{\omega_{x,y,z}}$, in roll, pitch, and yaw respectively. Such future experiments may validate or refute our assumption that individual conflicts do not vary by coordinate axes. It should be noted that Golding et al. conducted an experiment of this nature (Golding et al. 1995); however, subjects' heads were not restrained (received only a rear head support), and they conducted a visual search task inside a cabin.

Visual effects studies

Motion sickness for passive motions should also be assessed with and without visual cues (i.e., in the dark). This will inform whether the visual sensory conflicts (which may occur due to incongruence between the visual and vestibular cues) contribute to motion sickness. It is suggested that they do not, since individuals without a functioning vestibular system typically do not experience motion sickness (Golding 2016; Johnson et al. 1999; Murdin et al. 2015). In order to maintain congruency between the perceptual stage and experimental data, visual pathways must be included in the Observer model (Clark et al. 2019) for any modeling efforts leveraging experimental data with visual cues.

Future model advancements

Frequency effects

Following decades of experiments, it has been commonly accepted by researchers of motion sickness that there is a significant variation in severity across frequency, often peaking around 0.2 Hz. For upright vertical oscillations (e_{a_z} conflict) in an illuminated cabin, MSI was found to peak around 0.2 Hz in men (O'Hanlon and McCauley 1974). Similarly, fore-aft (x-axis) oscillations (a combination of e_a, e_ω, and e_f conflicts) in an illuminated cabin (while performing a visual search task and with the head not fully restrained) were shown to peak around 0.2 Hz (Golding et al. 2001). While undoubtedly crucial for understanding sea sickness from an operational perspective, these experiments are not applicable to this model because they do not meet the criteria of passive motions without visual cues (and as outlined in the introduction, modelers of motion sickness have not historically adhered to this understanding).

If experiments are able to quantify a frequency-motion sickness severity relationship for passive motions without visual cues, this relationship can be modeled by augmenting our proposed computational model. We propose two potential augmentations of this model. First, a representative filter (e.g., high, low, band pass, etc.) can be attached to the conflict terms feeding the neural mismatch signal. Alternatively (or in conjunction with this filter), the fast-pathway low-pass filter dynamics can be modified to no longer be critically damped. While Oman assumed the 2nd-order dynamics to be critically damped, others (Yunus et al. 2022a; b) have proposed using an underdamped system to augment the motion sickness severity dynamics. Doing so will expand the number of free parameters to include a damping ratio, and the model can be optimized with a new set of parameters.

Here we explore the frequency response of our model across OVAR rotation speeds at 30° tilt and for both earth-horizontal (e.g., y-axis) and earth-vertical (z-axis) translations. Denise et al. (1996) found peak sickness (minimum time to moderate nausea) to occur at chair speeds of 105 deg/s for 30° tilt (see Fig. 5). Compared to the Denise et al. (1996) data, our model performs well in the low frequency (<0.3 Hz) range but overpredicts the development of motion sickness at higher frequencies. One could remedy this by applying a low-pass filter (the first potential augmentation mentioned above) to the conflicts before weighting and combining the conflicts into the neural mismatch signal. To demonstrate this augmentation, an nth-order Butterworth low-pass filter was manually fit to match the model predictions to the Denise et al. (1996) data as an exploratory effort (filter parameters: $n = 8$ and $f_c = 0.34$ Hz). A corner frequency (f_c) above 0.3 Hz was chosen to minimize the impact of the filter on the training fit and preclude retraining the model. Our alternative approach (the second potential augmentation) was not explored here because a full re-fit of the set of model parameters would be required for this exploratory comparison.

While applying an ad hoc low-pass filter to match empirical data is consistent with the heuristic model of motion sickness for symptom dynamics, we caution that this filter is exploratory. Future works may explore how differences in the perceptual stage could circumvent the need for this modification; however, it is entirely possible that the CNS

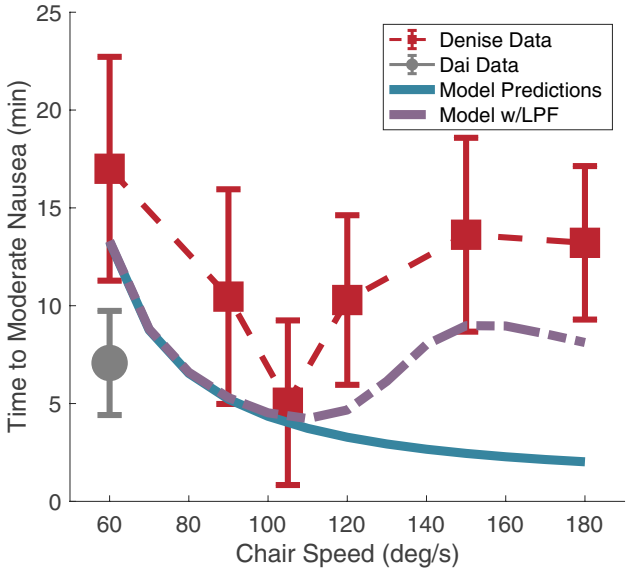

Fig. 5 Denise et al. (1996) empirical means (square shapes) and 95% confidence intervals are shown in red for OVAR motions, expressed as time to moderate nausea. All motions occurred at 30° of tilt. Also included are the Dai et al. (2010) empirical results with the mean (circle shape) and 95% confidence interval shown in gray (first converted to MISC, then time to MISC 7, roughly corresponding to moderate nausea). Model predictions (no filter) were made in this chair speed range, shown in blue (solid line). Model predictions with the inclusion of a low-pass conflict filter are shown in purple (dashed line). Model predictions are presented as time to MISC 7. The low-pass conflict filter was manually fit to the Denise et al. (1996) data

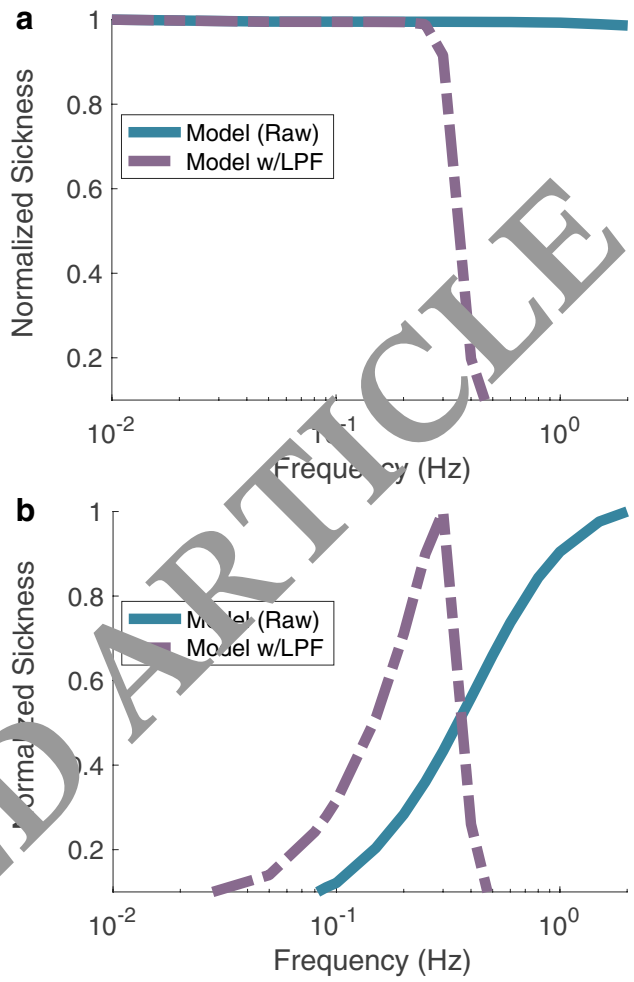

Fig. 6 Normalized sickness responses computed as the final predicted MISC after ten minutes of motion normalized by the peak sickness over the frequency range shown, with peak acceleration held constant between simulations. **a** Earth-vertical translational frequency response. **b** Earth-horizontal translational frequency response. Raw model predictions are shown in blue (solid line), and filtered-model predictions are shown in purple (dashed line)

employs low-pass filtering of the conflicts as explored here. Furthermore, the Denise et al. (1996) data has large uncertainty bounds, and the data collected by Dai et al. (2010) suggests a more rapid time to moderate nausea [and found peak sickness to occur at 60 deg/s for 30° of tilt, which we leveraged for training our model, provided in Fig. 3b]. Both Dai et al. (2010) and Denise et al. (1996) found faster chair velocities above 120 deg/s to result in less-severe motion sickness than lower chair velocities (mimicked with our model via the application of a low-pass conflict filter).

Resultant raw model (i.e., no ad hoc filter added) and filtered model predictions are additionally provided for earth-horizontal and earth-vertical translations in Fig. 6. For earth-vertical translations (Fig. 6a), peak sickness is largely constant for the raw model predictions and occurs in the 0.01 Hz to 0.2 Hz range for the filtered model predictions. Irmak et al. (2023) suggests that a variable estimate of the magnitude of gravity enables more frequency variability; however, it is unclear that the CNS would update its estimate of the magnitude of gravity during these motions. For earth-horizontal translations (Fig. 6b), peak sickness occurs around 1 Hz for the raw model predictions and around 0.3 Hz (near the low-pass filter cutoff frequency) for the filtered model predictions. Recently of note, Irmak et al. (2021) found the population-level susceptibility to motion sickness to be invariant during passive fore-aft motions in the dark at a peak acceleration amplitude of 2 m/s^2; however, the authors warn that this null finding may be due to the aggregation of individual differences over 23 subjects. If no population-level frequency effects are present, the above modifications can still be considered for modeling individual-level dynamics. Moreover, it is likely that the inclusion of other channels of sensory information (e.g., visual and active motion pathways) further augments these frequency response curves.

Visual effects and active motion effects

If visual sensory conflicts are found to not contribute to motion sickness, our model of motion sickness severity can be used to predict motion sickness with the presence of visual cues if the visual cues are sufficiently modeled using existing visual pathways in the Observer model (Clark et al. 2019; Newman 2009). Further, it is possible that the empirically observed frequency response naturally results from a validated visual Observer model with a cabin-fixed visual scene. Additionally, if an active pathway Observer model is developed without additional sensory conflict terms, our model and weights can be used to predict motion sickness for these motion paradigms as well [e.g., (Donohew and Griffin 2004, 2009; Griffin and Mills 2002b)]. This includes datasets which use active postural control to remain upright as well as Coriolis cross-coupled datasets which required subjects to perform active head tilts.

Modeling conflict processing and sickness dynamics with a recurrent neural network

While this proposed framework provides the first unified model of motion sickness based on the hypothesis that sensory conflict from self-orientation perception drives motion sickness, we recognize that the exact form of the sensory conflict processing and motion sickness dynamics are currently unknown. In future work, we propose training a recurrent neural network with the nine vestibular sensory conflict components over time as inputs and motion sickness reports as outputs. In this proposed approach, the Observer model of self-orientation perception will still drive the temporal dynamics of motion sickness, and new insights into the neural processing of sensory conflict and resultant motion sickness severity can be learned through explainable AI (Lundberg and Lee 2017). The same loss function proposed herein can and should be utilized to generate a mean population response model, and the loss from this future effort can be compared to assess model fit. In advance of this future modeling effort, more data should be collected for training purposes (in accordance with the experiments outlined in the "Suggested Future Experiments" section).

Appendix 1

Additional conflict information

See Table 1.

Table 1 contains descriptions of how various conflicts are realized within their respective models of self-orientation perception.

Table 1 Relevant sensory conflicts for driving motion sickness

Authors, year/model	Conflict name	Notation	Description
Merfeld et al. (1993)/observer model	Linear acceleration conflict	e_a	Vector difference between the 'sensed' GIF (f) and the centrally estimated GIF ($\hat{f}$). Units are g's
	GIF angle conflict	e_f	Vector perpendicular to f and $\hat{f}$, where the magnitude is radians between the two vectors
	Angular rate conflict	e_ω	Conflict between sensed and expected angular rate. Units are rad/s
Bos and Bles (1998)/SVC model	Vertical conflict	c	The scalar magnitude of the vector difference between the low-pass filtered otolith cues (i.e., pseudo- 'sensed' gravity) and the internal estimate of gravity
Khal[illegible] et al. (2001a, b)/SVH conflict model	Vertical conflict	c_v	Same as c in Bos
	Horizontal conflict	c_H	The scalar magnitude of the vector difference between the sensed gravito-inertial force vector normal to the Bos and Bles 'sensed' gravity and the internal estimate of the gravito-inertial force vector normal to the internal estimate of gravity
Wada et al./6-DoF	Vertical conflict	Δv	Same as c in Bos
Irmak et al. (2022)/no perceptual model	N/A (proportional to acceleration)	|a|	This conflict was not driven by a perceptual stage. Instead, conflict was assumed to be proportional to the absolute value of the acceleration of motion

Appendix 2

Additional dataset information

See Table 2 and Fig. 7.

Datasets considered for informing, training, or validating the model are described in Table 2. One dataset leveraged to train the model, Irmak et al. (2022) collected reports of motion sickness severity using the MISC scale in 17 subjects. The motion paradigm consisted of x-axis (fore-aft with subject seated upright) translation oscillations at 0.3 Hz beginning with up to 1 h of motion followed by a 10 min rest (no motion) and 30 min of additional oscillations. Many subjects were provided a unique, individualized sequence of motion vs. rest because a MISC report of 6 (moderate nausea) resulted in starting the rest period early. Subjects were tested across four amplitudes of oscillatory linear acceleration: 1.0, 1.5, 2.0, and 2.5 m/s^2. This study captures both motion amplitude and hypersensitivity effects [as outlined by Oman (Oman 1990)] and generates four conflicts (shown in Table 2 and Fig. 7). An additional dataset for training the model, Dai et al. (2010) performed the off-vertical axis rotation (OVAR) motion paradigm at 30° tilt and 60 deg/s rotation in 9 subjects (where individual response curves were provided). This motion paradigm offers a unique combination of conflicts compared to Irmak et al.'s dataset and captures motion sickness onset beyond an equivalent 6 (moderate nausea) on the MISC Scale, a key limitation outlined by Irmak et al.

Because neither individual subject responses over time nor averaged responses of all subjects over time were provided by Cian et al. (2011), this dataset was not used to train our model. However, we used it as a central-to-lower bound validation dataset. Furthermore, because Leger did not report subjects' temporal dynamics (i.e., they did not collect motion sickness reports over time during the onset of motion sickness symptoms), this dataset was also not used to train the model.

Table 2 Empirical datasets measuring motion sickness severity during passive motion in the dark, considered for tuning the model

Author, Year	Motion Paradigm	# Of Subjects	Subject Characteristic	Sensory Conflicts Present	Sickness Scale	Use
Irmak et al. 2022	Upright, x-axis oscillations for up to 1 hour, followed by a 10-minute rest and then a second motion phase lasting 30 minutes.	17	65th percentile MSSQ (mean) 2 F; 15 M	e_{a_x} e_{a_z} e_{ω_y} e_{f_y}	MISC	Training
Dai et al. 2010	OVAR, 30° tilt at 60 deg/s	9	<50th percentile MSSQ 5 F; 4 M	e_{a_x} e_{a_y} e_{ω_x} e_{ω_y} e_{ω_z} e_{f_x} e_{f_y} e_{f_z}	Simplified Pensacola Scale	Training
Cian et al. 2011	OVAR, 18° tilt, 72 deg/s	24	51st percentile MSSQ (mean) 12 M; 12 F	Same as Dai et al.	Six Point Scale	Validation
Leger et al. 1981	Earth-Horizontal Roll for up to 5 minutes	11	N/A MSSQ 14 M	e_{a_y} e_{a_z} e_{ω_x} e_{f_x}	Graybiel Scale	Inference of Weight Composition
Leger et al. 1981	Earth-Horizontal Pitch for up to 5 minutes	11	N/A MSSQ 14 M	e_{a_x} e_{a_z} e_{ω_y} e_{f_y}	Graybiel Scale	Inference of Weight Composition
Leger et al. 1981	Earth-Horizontal Yaw for up to 5 minutes	11	N/A MSSQ 14 M	e_{a_x} e_{a_y} e_{ω_z} e_{f_z}	Graybiel Scale	Inference of Weight Composition

Data used to train the model [Irmak et al. (2022) and Dai et al. (2010)] is shaded in white, data used to validated/assess the trained model (Cian et al.(2011)) is shaded in light gray, and data not used for quantitative comparison but instead used to draw insight (Leger et al. (1981)'s) three motion paradigms are shaded in dark gray

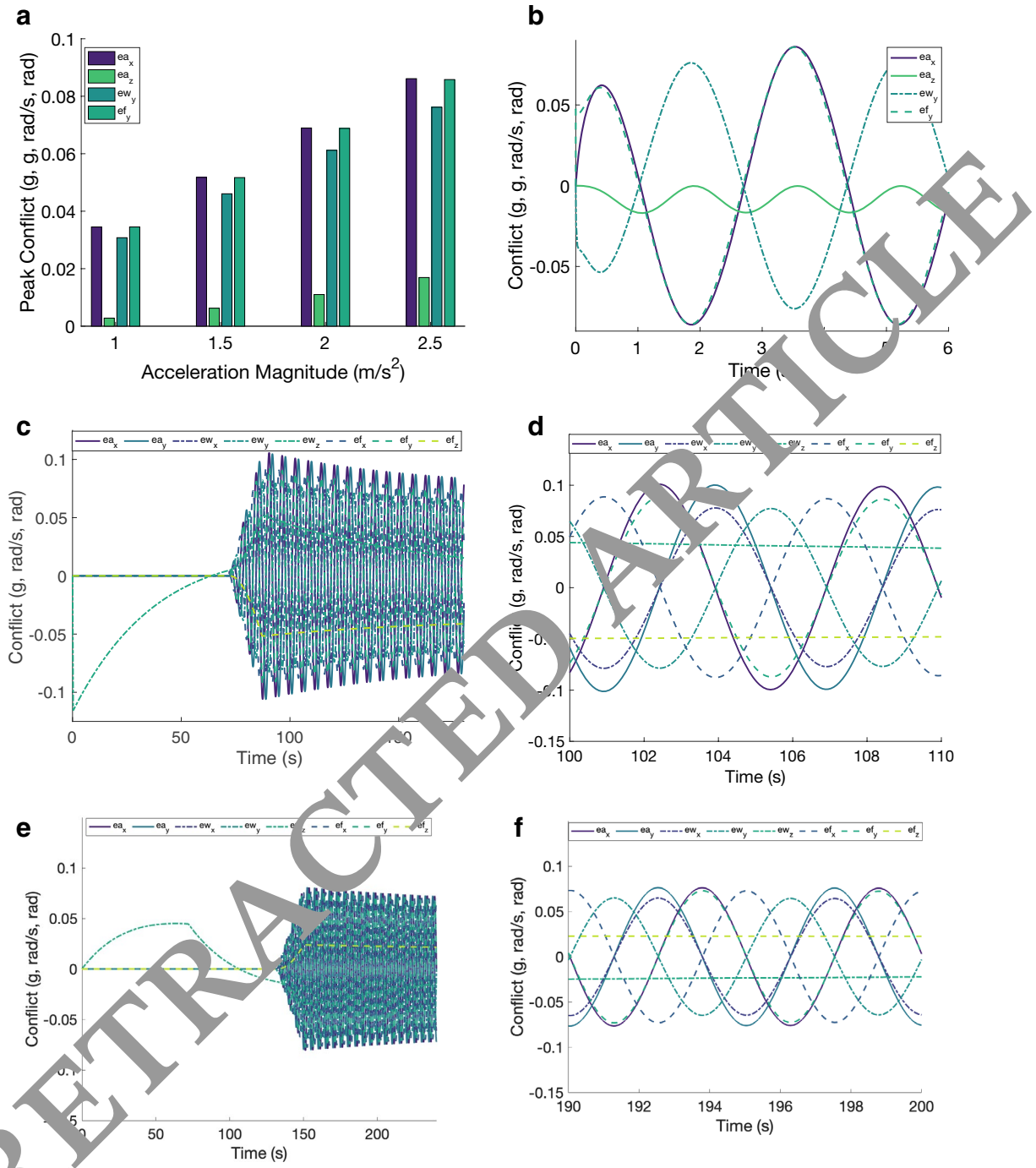

Fig. 7 **a** [illegible] conflict signals from Irmak et al.'s motion paradigm across acceleration amplitude **b** a representative steady sensory conflict signals from Irmak et al.'s motion paradigm at 2 m/s^2(conflict signal frequencies and phase shifts do not vary with acceleration amplitude)). OVAR sensory conflict signals of: **c** Dai et al. (2010)'s motion paradigm (first three minutes) **d** Dai et al. zoomed in. and **e** Cian et al. (2011)'s motion paradigm **f** Cian et al. (2011) zoomed in. For all plots, e_a conflicts are in units of g, e_ω conflicts are in units of rad/s, and e_f conflicts are in units of radians. All conflict types similarly scaled for these motions

Appendix 3

Additional optimization information

See Table 3 and Fig. 8.

Because the final cost found during optimization is dependent on the initial guess values for the free parameters, the optimization scheme may converge to local minima rather than an obvious global minimum. Unfortunately, our ability to perform many optimizations, with varying initial conditions, is limited because the optimization procedure is computationally expensive (69 Observer model and motion sickness dynamics simulations per function solution). We present our best solution, and the process for finding this best solution is described in more detail here. Notably, all instances of optimization (even outside these results), returned weights where $W_f \gg \{W_a, W_\omega\}$, with all three weight parameters yielding non-zero results.

Table 3 Summary of optimization results

Parameter	Optimize all		Units
	s_0 (initial)	s* (optimal)	
W_a	200	6.72	$1/g^2$
W_ω	200	11.7	$1/(rad/s)^2$
W_f	200	562	$1/rad^2$
K	70.4	91.2	ND
τ_f	66.2	73.8	s
τ_s	502.4	483	s
I_0	0	1e− 4	ND
n	0.4	0.323	ND
Final cost	–	3.587	

The solution found from optimizing all were considered but found to have a lower local minimum (final cost) than the parameters found from the transfer learning approach (grayed out set of parameters). Units are provided, and parameters corresponding to the relative symptom magnitude are left as non-dimensional (ND). For reference, the values used to initialize the optimization procedure are provided, which were the mean best-fit values from Irmak et al. (2022)

The model parameters providing the lowest cost were found by first optimizing all eight parameters until convergence was reached. Convergence was set to the default *fmincon* stopping criteria: a first-order optimality of 1e−6. Initial values were set to be Irmak et al.'s group-level median parameter values for the Oman's motion sickness symptom dynamics stage, zero for the threshold, and equal values of conflict weights. After convergence with all 8 training parameters, training was resumed considering just the three conflict weighting terms (W_a, W_ω and W_f) as free parameters until convergence was once again reached. This latter case is a transfer learning approach commonly used in machine learning. The initial and final values are presented in Table 3. The evolution of the cost and three conflict weighting terms over iterations is depicted in Fig. 8a. Before settling on the final values of the conflict weighting terms, the optimization routine considers a large range of combinations (Fig. 8b), thus alleviating some concerns about converging in local minima of the objective function.

Notable for predicting MISC resulting from vertical oscillations and gravity transitions, the W_a weighting term, which determines the contributions of the $|\overrightarrow{e_a}|$ conflict, fluctuated in the ~ 3 to 7 range across optimizations (depending on the initial conditions); modulating W_a in this range produces notable differences in MISC predictions but does little to affect the cost during optimization. Therefore, the best final value (producing the lowest cost and presented in Table 3)

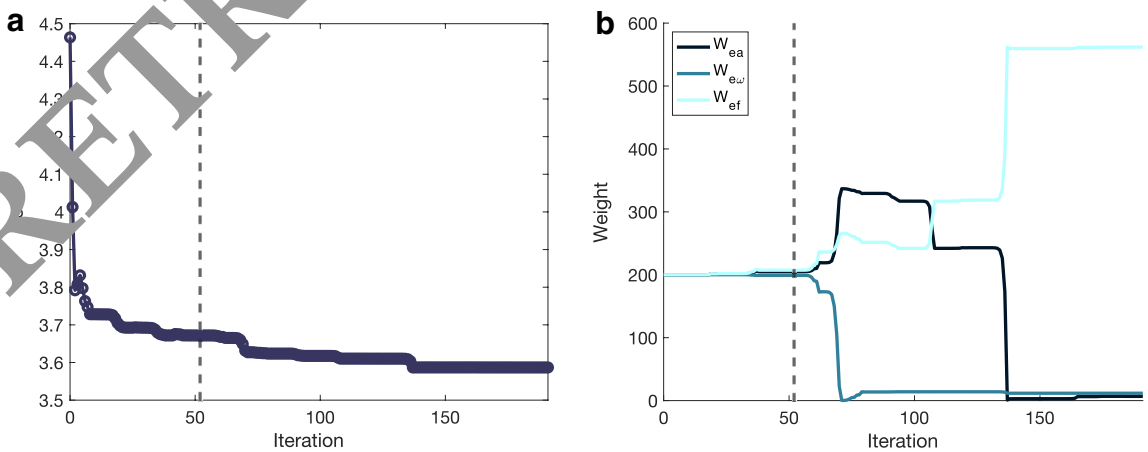

Fig. 8 **a** The evolution of the cost function over all iterations. **b** The evolution of the three conflict weighting terms over iterations. The three conflict weighting terms barely change during optimization of all eight parameters but eventually settle after the transfer learning stage where all parameters are frozen except for the three conflict weighting terms. The change from training all eight parameters to just the three conflict weighting terms occurred at the dashed-gray line

may underestimate or overestimate the true value due to the limits of the training dataset in isolating the $|\overrightarrow{e_a}|$ conflict.

We additionally explored training the model with only the W_a and W_ω weighting terms (setting W_f to zero) to see if the vector difference otolith and semi-circular canal sensory conflicts alone could sufficiently drive the temporal motion sickness dynamics. This was conducted after finding the best-fit presented herein as a post-hoc exploratory effort. This method yielded both a higher training cost ($J_{\mathrm{MMSE}} = 3.64$, in part likely due to a reduced number of free parameters) and worse qualitative predictions (found parameters were $W_a = 563$ $W_\omega = 0.25$) reinforcing the dependency of $|\overrightarrow{e_f}|$ when utilizing the Observer model.

Appendix 4

Additional training dataset results

See Fig. 9.

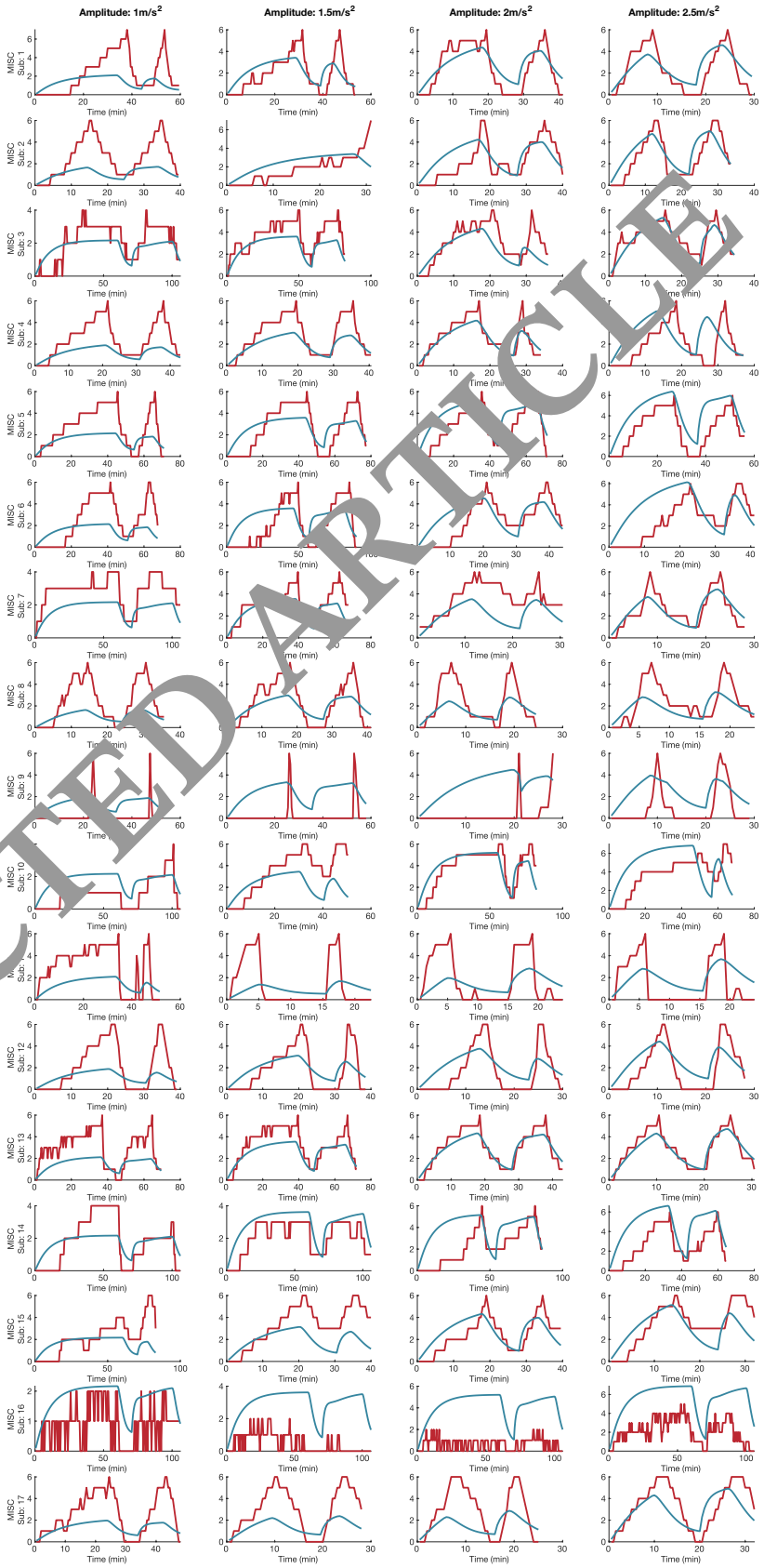

Fig. 9 Model PMSR predictions (blue) overlaying individual subject responses (red) from Irmak et al. (2022) across motion amplitudes

Comparisons to Irmak et al. (2022) for each subject across each motion amplitude are provided in Fig. 9. These comparisons are all made individually because most subjects received unique motion profiles (i.e., initial motion was often stopped after hitting a stopping criterion, and so motion resumed for most subjects at different time points). However, each model prediction remains a population mean symptom response prediction rather than an induvial response prediction, the latter of which is dependent on individuals' susceptibilities.

Acknowledgements Special thank you to Chuck Oman for his insightful feedback and ideas. We also acknowledge the authors who provided individual-level motion sickness severity reports in their publications, without which this effort would not have been possible.

Funding This work was supported by a NASA Space Technology Graduate Research Opportunities Award. Space Technology Mission Directorate, 80NSSC20K1202, Aaron Allred.

Data availability The final model is provided at https://github.com/aaronallred/Motion-Sickness-Dynamics. Additional datasets generated during and/or analyzed during the current study are available from the corresponding author on reasonable request.

Declarations

Conflict of interest The authors declare that they have no conflict of interest.

References

Bijveld MMC, Bronstein AM, Golding JF, Gresty MA (2008) Nauseogenicity of off-vertical axis rotation vs. equivalent visual motion. Aviat Space Environ Med 79(7):665. https://doi.org/10.3357/ASEM.2241.2008

Bos JE (2011) Nuancing the relationship between motion sickness and postural stability. Displays 32(4):189–193. https://doi.org/10.1016/j.displa.2010.09.005

Bos JE, Bles W (1998) Modelling motion sickness and subjective vertical mismatch detailed for vertical motions. Brain Res Bull 47(5):537–542. https://doi.org/10.1016/S0361-9230(98)00088-4

Bos JE, MacKinnon SN, Patterson A (2005) Motion sickness symptoms in a ship motion simulator: effects of inside, outside, and no view. 76(12):8

Bos JE, Bles C, Graman JL (2022) Beyond seasickness: a motivated call for a new motion sickness standard across motion environments. Vibration 5(4):755–769. https://doi.org/10.3390/vibration5040044

Brooks JX, Cullen KE (2009) Multimodal integration in rostral fastigial nucleus provides an estimate of body movement. J Neurosci 29(34):10499–10511. https://doi.org/10.1523/JNEUROSCI.1937-09.2009

Cian C, Ohlmann T, Ceyte H, Gresty MA, Golding JF (2011) Off vertical axis rotation motion sickness and field dependence. Aviat Space Environ Med 82(10):959–963. https://doi.org/10.3357/ASEM.3049.2011

Clark TK, Newman MC, Karmali F, Oman CM, Merfeld DM (2019) Mathematical models for dynamic, multisensory spatial orientation perception. Progress in brain research, vol 248. Elsevier, Amsterdam, pp 65–90. https://doi.org/10.1016/bs.pbr.2019.04.014

Dai M, Kunin M, Raphan T, Cohen B (2003) The relation of motion sickness to the spatial temporal properties of velocity storage. Exp Brain Res 151(2):173–189. https://doi.org/10.1007/s00221-003-1479-4

Dai M, Sofroniou S, Kunin M, Raphan T, Cohen B (2010) Motion sickness induced by off-vertical axis rotation (OVAR). Exp Brain Res 204(2):207–222. https://doi.org/10.1007/s00221-010-2305-4

Davis JR, Vanderploeg JM, Santy PA, Jennings RT, Stewart DF (1988) Space motion sickness during 24 flights of the space shuttle. Aviat Space Environ Med 59(12):1185–1189

de Winkel KN, Irmak T, Kotian V, Pool DM, Happee R (2021) Relating individual motion sickness levels to subjective discomfort ratings. Exp Brain Res 240(4):1231–1240. https://doi.org/10.1007/s00221-022-06334-6

Denise P, Etard O, Zupan L, Darlot C (1996) Motion sickness during off-vertical axis rotation: prediction by a model of sensory interactions and correlation with other forms of motion sickness. Neurosci Lett 202(3):183–186. https://doi.org/10.1016/0304-3940(96)12302-2

Donohew BE, Griffin MJ (2004) Motion sickness: effect of the frequency of lateral oscillation. 75(8):8

Donohew BE, Griffin MJ (2009) Motion sickness with fully roll-compensated lateral oscillation: effect of oscillation frequency. Aviat Space Environ Med 80(2):94–101. https://doi.org/10.3357/ASEM.2345.2009

Golding JF (2016) Motion sickness. Handbook of clinical neurology, vol 137. Elsevier, Amsterdam, pp 371–390. https://doi.org/10.1016/B978-0-444-63437-5.00027-3

Golding JF, Phil D, Markey HM, Stott RR (1995) The effects of motion direction, body axis, and posture on motion sickness induced by low frequency linear oscillation. Aviat Space Environ Med 66(11):1046

Golding JF, Mueller A, Gresty M (2001) A motion sickness maximum around the 0.2 Hz frequency range of horizontal translational oscillation. Aviat Space Environ Med 72(3):188–192

Griffin MJ, Mills KL (2002a) Effect of frequency and direction of horizontal oscillation on motion sickness. Aviat Space Environ Med 73(6):537–543

Griffin MJ, Mills KL (2002b) Effect of magnitude and direction of horizontal oscillation on motion sickness. Aviat Space Environ Med 73(7):640–646

Groen EL, Clark TK, Houben MMJ, Bos JE, Mumaw RJ (2022) Objective evaluation of the somatogravic illusion from flight data of an airplane accident. Safety. https://doi.org/10.3390/safety8040085

Guedry FE, Benson AJ, Moore HJ (1982) Influence of a visual display and frequency of whole-body angular oscillation on incidence of motion sickness. Aviat Space Environ Med 53(6):564–569

Hainich R, Drewitz U, Ihme K, Lauermann J, Niedling M, Oehl M (2021) Evaluation of a human-machine interface for motion sickness mitigation utilizing anticipatory ambient light cues in a realistic automated driving setting. Information. https://doi.org/10.3390/info12040176

Heer M, Paloski WH (2006) Space motion sickness: incidence, etiology, and countermeasures. Auton Neurosci 129(1–2):77–79. https://doi.org/10.1016/j.autneu.2006.07.014

Irmak T, de Winkel KN, Pool DM, Bülthoff HH, Happee R (2021) Individual motion perception parameters and motion sickness frequency sensitivity in fore-aft motion. Exp Brain Res 239(6):1727–1745. https://doi.org/10.1007/s00221-021-06093-w

Irmak T, Kotian V, Happee R, de Winkel KN, Pool DM (2022) Amplitude and temporal dynamics of motion sickness. Front Syst Neurosci 16:866503. https://doi.org/10.3389/fnsys.2022.866503

Irmak T, Pool DM, De Winkel KN, Happee R (2023) Validating models of sensory conflict and perception for motion sickness prediction. Biol Cybern. https://doi.org/10.1007/s00422-023-00959-8

Jamali M, Sadeghi SG, Cullen KE (2009) Response of vestibular nerve afferents innervating utricle and saccule during passive and active translations. J Neurophysiol 101(1):141–149. https://doi.org/10.1152/jn.91066.2008

Johnson WH, Mayne JW (1953) Stimulus required to produce motion sickness; restriction of head movement as a preventive of airsickness; field studies on airborne troops. J Aviat Med 24(5):400–411

Johnson WH, Sunahara FA, Landolt JP (1999) Importance of the vestibular system in visually induced nausea and self-vection. J Vestib Res 9(2):83–87. https://doi.org/10.3233/VES-1999-9202

Kamiji N, Kurata Y, Wada T, Doi S (2007) Modeling and validation of carsickness mechanism. SICE Ann Conf 2007:1138–1143. https://doi.org/10.1109/SICE.2007.4421156

Karjanto J, Md Yusof N, Wang C, Terken J, Delbressine F, Rauterberg M (2018) The effect of peripheral visual feedforward system in enhancing situation awareness and mitigating motion sickness in fully automated driving. Transp Res Part F: Traffic Psychol Behav 58:678–692. https://doi.org/10.1016/j.trf.2018.06.046

Khalid H, Turan O, Bos JE (2011a) Theory of a subjective vertical–horizontal conflict physiological motion sickness model for contemporary ships. J Mar Sci Technol 16(2):214–225. https://doi.org/10.1007/s00773-010-0113-y

Khalid H, Turan O, Bos JE, Incecik A (2011b) Application of the subjective vertical–horizontal-conflict physiological motion sickness model to the field trials of contemporary vessels. Ocean Eng 38(1):22–33. https://doi.org/10.1016/j.oceaneng.2010.09.008

Kolasinski EM (1995) Simulator sickness in virtual environments US Army Research Institute for the Behavioral and Social Sciences

Kravets VG, Dixon JB, Ahmed NR, Clark TK (2021) COMPASS: computations for orientation and motion perception in altered sensorimotor states. Fronti Neural Circuits. https://doi.org/10.3389/fncir.2021.757817

Kravets VG, Ahmed N, Clark TK (2022) A Rao-Blackwellized particle filter for modeling neurovestibular adaptation to altered gravity. In: 51st International Conference on Environmental Systems. St Paul, MN

Kuiper OX, Bos JE, Diels C, Schmidt EA (2020a) Knowing what's coming: anticipatory audio cues can mitigate motion sickness. Appl Ergonom 85:103068. https://doi.org/10.1016/j.apergo.2020.103068

Kuiper OX, Bos JE, Schmidt EA, Diels C, Wolter S (2020b) Knowing what's coming: unpredictable motion cues increase motion sickness. Human Fact: J Human Fact Ergonom Soc 62(8):1339–1348. https://doi.org/10.1177/0018720819876139

Lackner JR (2014) Motion sickness: more than nausea and vomiting. Exp Brain Res 232(8):2493–2510. https://doi.org/10.1007/s00221-014-4008-5

Lackner JR, Graybiel A (1987) Head movements in low and high gravitoinertial force environments elicit motion sickness: implications for space motion sickness. Aviat Space Environ Med 58(9 Pt 2):A211–217

Lackner JR, DiZio P (2006) Space motion sickness. Exp Brain Res 175(3):377–399. https://doi.org/10.1007/s00221-006-0697-y

Laurens J (2022) The otolith vermis: a systems neuroscience theory of the nodulus and Uvula. Front Syst Neurosci. https://doi.org/10.3389/fnsys.2022.886284

Lawson BD (2014) Chapter 24. Motion Sickness Scaling. In: Handbook of Virtual Environments, pp. 601–626

Leger A, Money KE, Landolt JP, Cheung BS, Rodden BE (1981) Motion sickness caused by rotations about Earth-horizontal and Earth-vertical axes. J Appl Physiol 50(3):469–477. https://doi.org/10.1152/jappl.1981.50.3.469

Li D, Chen L (2022) Mitigating motion sickness in automated vehicles with vibration cue system. Ergonomics 65(10):1313–1325. https://doi.org/10.1080/00140139.2022.2028902

Luenberger D (1971) An introduction to observers. IEEE Trans Autom Control 16(6):596–602. https://doi.org/10.1109/TAC.1971.1099826

Lundberg S, Lee S.-I (2017) A unified approach to interpreting model predictions. [Cs, Stat]. http://arxiv.org/abs/1705.07874. Accessed 28 Feb 2021

Mayne R (1974) A systems concept of the vestibular organs. In: Kornhuber HH (ed) Vestibular system part 2: psychophysics, applied aspects and general interpretations, vol 6/2. Springer, Berlin, Heidelberg, pp 493–580. https://doi.org/10.1007/978-3-642-65920-1_14

Merfeld DM, Young LR, Oman CM, Shelhamert MJ (1993) A multidimensional model of the effect of gravity on the spatial orientation of the monkey. J Vestib Res 3(2):141–161. https://doi.org/10.3233/VES-1993-3204

Mills KL, Griffin MJ (2000) Effect of seating, motion and direction of horizontal oscillation on motion sickness. Aviat Space Environ Med 71(10):996–1002

Murdin L, Chamberlain F, Cheema S, Arshad Q, Gresty MA, Golding JF, Bronstein A (2015) Motion sickness in migraine and vestibular disorders: figure 1. J Neurol Neurosurg Psychiatry 86(5):585–587. https://doi.org/10.1136/jnnp-2014-308331

Newman MC (2009) A multisensory observer model for human spatial orientation perception. Massachusetts Institute of Technology

O'Hanlon J, McCauley J (1974) Motion sickness incidence as a function of vertical sinusoidal motion.pdf. Aerosp Med Human Perform 45:366–369

Oman CM (1982) A heuristic mathematical model for the dynamics of sensory conflict and motion sickness. https://go.exlibris.link/rJjgfgfW

Oman CM (1987) Spacelab experiments on space motion sickness. Acta Astronaut 15(1):55–66. https://doi.org/10.1016/0094-5765(87)90066-X

Oman CM (1990) Motion sickness: A synthesis and evaluation of the sensory conflict theory. Can J Physiol Pharmacol 68(2):294–303. https://doi.org/10.1139/y90-044

Oman CM, Cullen KE (2014) Brainstem processing of vestibular sensory exafference: Implications for motion sickness etiology. Exp Brain Res 232(8):2483–2492. https://doi.org/10.1007/s00221-014-3973-2

Ortega HJ, Harm DL, Reschke MF (2019) Space and entry motion sickness. In: Barratt MR, Baker ES, Pool SL (eds) Principles of clinical medicine for space flight. Springer New York, New York, pp 441–456. https://doi.org/10.1007/978-1-4939-9889-0_14

Reason JT, Brand JJ (1975) Motion sickness, vol vii. Academic Press, Cambridge, p 310

Reuten AJC, Nooij SAE, Bos JE, Smeets JBJ (2021) How feelings of unpleasantness develop during the progression of motion sickness symptoms. Exp Brain Res 239(12):3615–3624. https://doi.org/10.1007/s00221-021-06226-1

Riccio GE, Stoffregen TA (1991) An ecological theory of motion sickness and postural instability. Ecol Psychol 3(3):195–240. https://doi.org/10.1207/s15326969eco0303_2

Roy JE, Cullen KE (2004) Dissociating self-generated from passively applied head motion: neural mechanisms in the vestibular nuclei. J Neurosci 24(9):2102–2111. https://doi.org/10.1523/JNEUROSCI.3988-03.2004

Turan O, Verveniotis C, Khalid H (2009) Motion sickness onboard ships: Subjective vertical theory and its application to full-scale trials. J Mar Sci Technol 14(4):409–416. https://doi.org/10.1007/s00773-009-0064-3

Wada T, Fujisawa S, Doi S (2018) Analysis of driver's head tilt using a mathematical model of motion sickness. Int J Ind Ergon 63:89–97. https://doi.org/10.1016/j.ergon.2016.11.003

Wada T, Kawano J, Okafuji Y, Takamatsu A, Makita M (2020) A computational model of motion sickness considering visual and vestibular information. 2020 IEEE International Conference on Systems, Man, and Cybernetics (SMC), 1758–1763. https://doi.org/10.1109/SMC42975.2020.9283350

Wolpert DM, Ghahramani Z, Jordan MI (1995) An internal model for sensorimotor integration. Science 269(5232):1880–1882. https://doi.org/10.1126/science.7569931

Yunus I, Farhan Witjaksono F, Naz Başokur E, Jerrelind J, Drugge L (2022a) Analysis of human perception models for motion sickness in autonomous driving. 13th International Conference on Applied Human Factors and Ergonomics (AHFE 2022a). https://doi.org/10.54941/ahfe1002473

Yunus I, Jerrelind J, Drugge L (2022b) Evaluation of motion sickness prediction models for autonomous driving. In: Orlova A, Cole D (eds) Advances in dynamics of vehicles on roads and tracks II. Springer International Publishing, Cham, pp 875–887. https://doi.org/10.1007/978-3-031-07305-2_81

Zupan LH, Merfeld DM, Darlot C (2002) Using sensory weighting to model the influence of canal, otolith and visual cues on spatial orientation and eye movements. Biol Cybern 86(3):209–230. https://doi.org/10.1007/s00422-001-0290-1